Lu Han[a], Premkumar Kamalanathan and Muthanna H. Al-Dahhan*

Gas–liquid mass transfer using advanced optical probe in a mimicked FT slurry bubble column

https://doi.org/10.1515/ijcre-2020-0143
Received August 18, 2020; accepted December 12, 2020;
published online December 25, 2020

Abstract: Gas-liquid volumetric liquid-phase mass transfer coefficient (k_La) was studied in a slurry bubble column at the conditions mimicking Fischer–Tropsch synthesis. To avoid the hydrodynamic disturbances due to the gas switching, oxygen enriched air dynamic absorption method was used. Influence of reactor models (CSTR, ADM and RCFD) on the volumetric mass transfer coefficient was investigated. Effect of operating pressure, superficial gas velocity and solids loading were investigated. From the reactor models investigated, it is recommended to use ADM model for k_La study. If the CSTR model is used, applicability of the model should be checked. With increase in the superficial gas velocity and operating pressure, volumetric liquid-phase mass transfer coefficient increases, while it decreases with the solids loading corroborating with the literature.

Keywords: dissolved oxygen optical probe; slurry bubble column; mass transfer coefficient.

1 Introduction

Fischer–Tropsch (FT) synthesis converts the syngas from coal/biomass/natural gas to the more useful synthetic fuels and precursors. For the commercial scale FT synthesis, slurry bubble column reactor (SBCR) is the widely accepted choice of the reactor. SBCR is a three phase reactor, where the syngas is sparged in the form of bubbles through the slurry of FT wax and catalysts. The syngas from bubbles has to diffuse through the interfaces (gas–liquid, liquid–solid) and bulk liquid to reach the active catalyst site where the reaction happens. Out of these, the gas to liquid transport is the limiting step in FT-SBCR (Basha et al. 2015; Jin et al. 2014). Thus, the volumetric liquid-phase mass transfer coefficient (k_La) that characterizes the gas to liquid mass transport plays a decisive role in the performance of the FT-SBCR. Table 1 gives the literature on k_La studies available at the physical properties of phases relevant to the FT synthesis. From the table it can be inferred that only few studies (Behkish et al. 2002; Sehabiague and Morsi 2013) were available *at the conditions* relevant to the industrial FT synthesis, other studies were either conducted at ambient pressure or at low velocity conditions (<0.1 m/s), *thus warranting more studies on* the volumetric liquid-phase mass transfer coefficient (k_La).

The volumetric liquid-phase mass transfer coefficient is experimentally measured using dynamic absorption techniques or reactive (chemical reactions) techniques in the literature (Jin et al. 2014; Li and Zhu 2016; Sehabiague and Morsi 2013). Due to its simplicity and wide applicability, dynamic gas absorption/desorption method was used widely (Table 1). In dynamic gas absorption/desorption method, the rate of change of concentration of the gas is recorded immediately after switching the gas of interest from the inert gas or vice-versa. The process of switching disturbs the hydrodynamics, thus affecting the measurement of k_La. Further, this method has the disadvantage of large volume of gas required. To overcome the disadvantages of conventionally used dynamic absorption technique, oxygen enriched air method was used in this work. Previously, this method was used in biochemical reactors (Chang, Halard, and Moo-Young 1989; Linek, Sinkule, and Benes 1991), bubble column (Han and Al-Dahhan 2007) and bubble column photo bioreactor (Manjrekar et al. 2017). In this method, a small oxygen flow is added to the existing air flow, thus making effective switching without disturbing the hydrodynamics and only small volume of oxygen gas required for the measurement. The concentration of oxygen was measured using the dissolved oxygen optical probe in this work. Dissolved oxygen optical probe is widely used due to the faster response, higher sensitivity, higher

[a] Presently in ExxonMobil Research and Engineering, Annandale, NJ, USA.

***Corresponding author: Muthanna H. Al-Dahhan**, Chemical Reaction Engineering Laboratory, Washington University, St Louis, MO 63130, USA; and Department of Chemical and Biochemical Engineering, Missouri University of Science and Technology, Rolla, MO 65409, USA, E-mail: aldahhanm@mst.edu

Lu Han, Chemical Reaction Engineering Laboratory, Washington University, St Louis, MO 63130, USA

Premkumar Kamalanathan, Department of Chemical and Biochemical Engineering, Missouri University of Science and Technology, Rolla, MO 65409, USA. https://orcid.org/0000-0001-9425-8675

Table 1: Studies on the volumetric mass transfer coefficient in the SBCR at physical properties of phases relevant to FT synthesis.

References	Phases			D, m	Operating conditions				Experimental technique
	Gas	Liquid	Solid		U_G, m/s	C_s, vol%	P, MPa	T, K	
Deckwer et al. (1980)	N_2, CO	Paraffin	Al_2O_3	0.04, 0.1	0.01–0.036	16 wt%	1.1	416, 543	Chemical reaction
Yang, Wang, and Jin (2001)	H_2/CO	Paraffin	Silica gel	0.037	0.0025–0.02	5–20	1–5	293–523	Dynamic desorption
Behkish et al. (2002)	H_2, O, N_2, CH_4	Isopar-m, hexanes	Glass beads, iron oxide	0.3	0.085–0.39	0–36	3	473	Transient physical gas absorption
Vandu and Krishna (2004)	Air/O_2	Paraffin, water, tetradecane, ethanol, tellus oil	Silica	0.1	0.03–0.4	0–25	Atm	Atm	Dynamic absorption
Vandu, Koop, and Krishna (2004)	Air/O_2	C9C11	Alumina catalyst – porous	0.1	0.03–0.4	0–25	Atm	Atm	Dynamic absorption
Ghani, Yacup, and Saleh (2012)	O_2	C10C13	Alumina/silica powders	0.1 × 0.02	0.01–0.12	5	Atm	Atm	Dynamic absorption
Sehabiague and Morsi (2013)	He,N_2	Paraffin, light, heavy FT cut	Alumina, puralox alumina, iron oxide	0.29	0.14–0.26	3–20	8–30	330–530	Transient physical gas absorption
Jin et al. (2014)	H_2, CO, CO_2	Paraffin	Sand	0.1	0.03–0.1	0–20 wt%	1–3	293–473	Dynamic absorption
Abdul Kareem, Gheni, and Yacoup (2016)	O_2	C9C11	Silica	0.1 × 0.07	0.02–0.08	0–25	Atm	Atm	Dynamic absorption

precision, ease of use, stability, ability to use in harsh environments, etc. (Wei et al. 2019). The disadvantages of dissolved oxygen optical probe are chances of physical damage of the film, mechanical abrasion and fouling (Zhang et al. 2019). Previously, dissolved oxygen probe has been used successfully in various two and three-phase applications (Jordan et al. 2002; Lau et al. 2004; Wei et al. 2019; Zhang et al. 2019), including slurry bubble column containing solids upto 50 vol% (Ghani, Yacup, and Saleh 2012; Vandu, van den Berg and Krishna 2005). Due to the advantages of the dissolved oxygen probe and proven applicability in SBCR, it is used in this work.

In SBCR, the rate of change of concentration measured in the reactor can be due to the mass transfer as well as the mixing in the reactor. Mixing depends on the flow characteristics in the reactor. Hence, mixing in the column should be modeled with appropriate reactor models to obtain the mass transfer coefficient. This is especially important for the measurements using the point probes. The CSTR model was used by most of the researchers, where uniform mixing was assumed. Few researchers used one-dimensional ADM model and reported significant differences in the mass transfer coefficient between ADM and CSTR model (Deckwer et al. 1983; Gourich et al. 2008; Han and Al-Dahhan 2007; Lau et al. 2004). In the 1-D ADM, large scale recirculation and dispersion in the SBCR is lumped together in a single parameter of effective dispersion coefficient. That is, ADM model is over simplified representation of flow in SBCR. Based on the liquid recirculation in bubble column and velocity field in bubble column, Degaleesan et al. (1996) proposed a phenomenological model called as RCFD (recirculation and cross flow with dispersion). RCFD represents the physical phenomena in SBCR better than ADM by decoupling the global recirculation. RCFD is a compartment model, where four compartments are assumed, viz., upflow, downflow, sparger and disengagement zone. Sparger and disengagement zones are modeled as CSTR, meanwhile upflow and downflow zones are modeled as the ADM with cross flow dispersion between them. Previous studies confirmed that the RCFD model predicted the tracer responses well during the methanol, FT and dimethyl ether synthesis (Chen et al. 2006; Degaleesan 1997; Gupta et al. 2001). Even though the previous studies compared the effect of using ADM and CSTR on k_La, it remains to be tested how this phenomenological model (RCFD) performs. Such a comparative study is important for the use of such model in SBCR, as it is known that the inappropriate/wrong model greatly affects the results (Deckwer et al. 1983). Thus, the principal objective of this work is a comparative study of CSTR, ADM and RCFD model, where the model parameters of

dispersion, holdup, and velocity are experimentally obtained rather than values from the correlations as in most of the previous studies. It is to be noted that the relatively less use of ADM and other models for the k_La measurement is due to the need of dispersion and phase holdup required *a priori*. In this work, dispersion, velocity and phase holdup required were obtained from our previous studies at the same conditions in the same column. With the results of comparative study, an attempt has been made to explain the contradictory results in the literature on the variation of k_La with axial sampling position.

The other objective of this work is to study the volumetric liquid-phase mass transfer coefficient at the operating conditions of the previous work to generate comprehensive data. For the design of FT-SBCR, availability of the design parameters like phase distribution, velocities, dispersion, mass and heat transfer coefficient at the similar conditions will facilitate a more reliable model. Moreover, such a comprehensive data will be invaluable for the CFD model development and validation. However, such a comprehensive data are not available, even though few studies reported the bubble dynamics and k_La at the similar conditions (Jin et al. 2014; Sehabiague and Morsi 2013; Yang, Wang, and Jin 2001). As a part of ongoing effort to generate the comprehensive data in the high pressure SBCR for FT synthesis in this lab, phase holdup, bubble dynamics, solid dynamics, gas, liquid and solid dispersion were studied previously at the similar conditions (Han 2007; Han, Said, and Al-Dahhan 2018; Shaikh 2007; Wu 2007; Wu, Suddard, and Al-Dahhan 2008). In this work, volumetric liquid-phase mass transfer coefficient was studied at the similar conditions of the previous work to generate comprehensive data.

2 Experimental

2.1 Experimental setup

Figure 1 shows the schematic of experimental setup used. Slurry bubble column reactor (SBCR) used in this work is made of stainless steel. The inner diameter of SBCR is 0.162 m and length is 2.52 m. A perforated plate was used as a gas distributor. The distributor has totally 163 holes of 1.32 mm diameter arranged in a triangular pitch with open area of 1.3%. The threaded ports were made available on the wall of the SBCR, which facilitated the probe insertion for the measurements. Backpressure regulator provided in the outlet line was used to control the pressure. Safety valves were provided to ensure the safe operation. Gas, liquid and solids were carefully selected to mimic the FT synthesis at the room temperature. At the pressure of 1 MPa, the density of air (11.8 kg/m^3) is similar to the syngas of low temperature FT process. Similarly, the properties of hydrocarbon mixture of C9–C11 compounds supplied by Sasol mimics the FT wax. This hydrocarbon mixture is referred as C9C11 (ρ_L – 728 kg/m^3, μ_L – 0.00084 Pa s, σ – 0.0232 N/m) in this work. The inert, porous, alumina FT catalyst skeleton (mean diameter – 75 μm) was used as solid phase. This catalyst skeleton is similar in size, density and porosity of the active FT catalyst. Liquid and solids were loaded from the top and unloaded through the drain valve at the bottom. Air was supplied by the compressors through the filters. Rotameters were used to meter the flow rate. Dynamic height of the aerated slurry was maintained at 1.8 m. The experimental conditions studied in this work is given in Table 2.

2.2 Measurement technique

Optical oxygen probe manufactured by Ocean Inc. was used to measure the dissolved oxygen concentration. This probe consists of light source, optical fiber, thin film consisting of fluorescent molecules coated on the probe tip, spectrometer, USB A/D converter and computer. The working principle of this fluorescence type sensor is as follows. Light source emits 475 nm wavelength light on the thin film coated on the tip of the probe, which in turn emits the 600 nm wavelength light. The dissolved oxygen interacts with the fluorescent molecules, thus interfering in the emission process resulting in the reduction of intensity of the 600 nm wavelength light emitted. This process is called 'quenching'. The intensity reduced is linearly proportional to the dissolved oxygen concentration. The intensity of the light was measured by spectrometer, which was connected to the computer for data acquisition. The measured concentration (C_p) of the dissolved oxygen at time t differs from actual concentration of the oxygen $C_L(t)$ in the liquid due to the delay in the response time of the probe. This delay is typically modeled as first order process (Gourich et al. 2008; Jin et al. 2014),

$$\frac{dC_p(t)}{dt} = k_p\left(C_L(t) - C_p(t)\right) \tag{1}$$

where k_p is the probe constant. The probe constant, k_p, was obtained by conducting experiments as follows. Two containers of liquid – one saturated with oxygen by air flow and other one stripped of oxygen by supply of nitrogen gas – were used. Optical fiber probe kept in the container of oxygen stripped liquid was immediately moved to the container of oxygen saturated liquid, thereby a step change

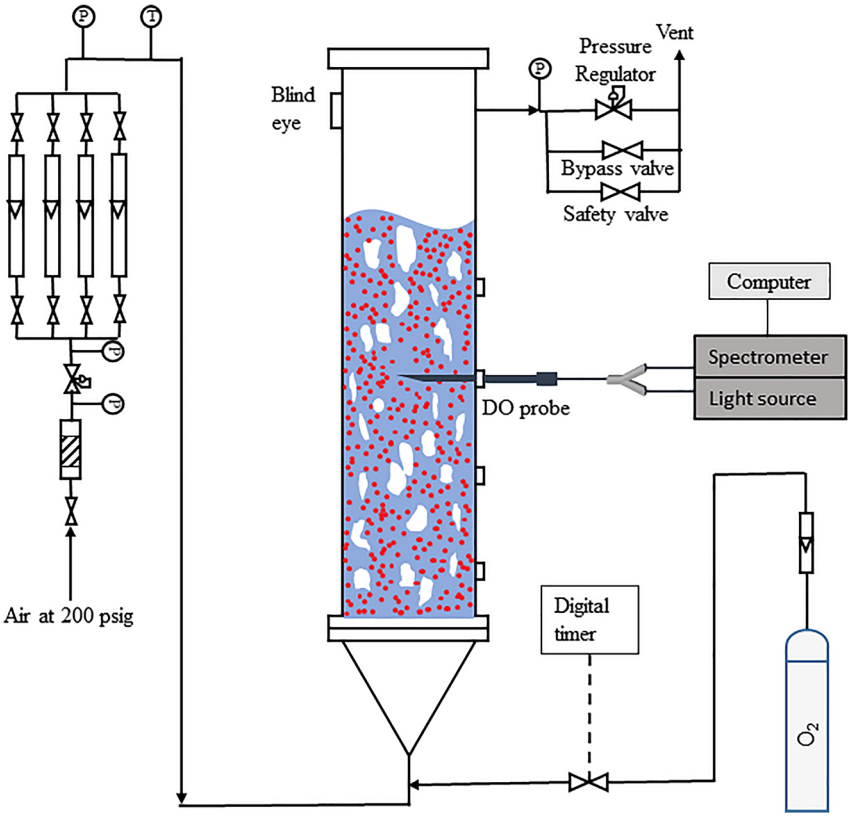

Figure 1: Schematic of slurry bubble column reactor (SBCR) experimental setup used for measuring dissolved oxygen by optical oxygen probe.

of concentration was imposed. The yielded response gives the actual DO concentration after a delay k_p which can be computed by integrating eq. (1) with the initial conditions of $t = 0$, $C_L(t) = 0$, which results in

$$C_p(t) = C^*_{L,A}\left(1 - e^{-k_p t}\right) \tag{2}$$

The actual response (Figure 2) was fitted using eq. (2) to obtain the probe constant. From the fitting, k_p was found to be 1.1 s^{-1}.

As explained earlier, oxygen enriched air dynamic absorption technique was used in this work to avoid the hydrodynamic disturbance. To inject the oxygen in the stream of airflow, provisions were made on the air line just before the plenum as shown in Figure 1. The oxygen was supplied from the cylinder. The oxygen flow rate of 3% of total flow rate was added by using solenoid value synchronized with the digital timer. To avoid the influence of noises due to the relatively small quantity of the oxygen, experiments were repeated until the average of all the experiments gave the smooth curve with less noise. The smoothened curve were used for the further processing. The actual DO concentration in the liquid can be obtained by rewriting eq. (1) as,

$$C_L(t) = C_p(t) + \frac{1}{k_p}\frac{dC_p(t)}{dt} \tag{3}$$

The radial position of the probe was kept at the center ($r/R = 0$) of the column for the axial dispersion model (ADM) and at both $r/R = 0$ and $r/R = 0.85$ for the mechanistic RCFD model.

Table 2: Experimental conditions of oxygen mass transfer measurements.

System	Superficial gas velocity U_G, m/s	Pressure, MPa	Solids loading, C_s
Air-C_9C_{11}-FT catalyst	0.03, 0.05, 0.08, 0.14, 0.20, 0.30	1.0	0
		0.1	0
		1.0	9.1 vol%
		0.1	9.1 vol%
		1.0	25 vol%
		0.1	25 vol%

3 Theoretical background

3.1 CSTR model

With the assumption of perfect mixing, change in the concentration of oxygen in the liquid phase is given by,

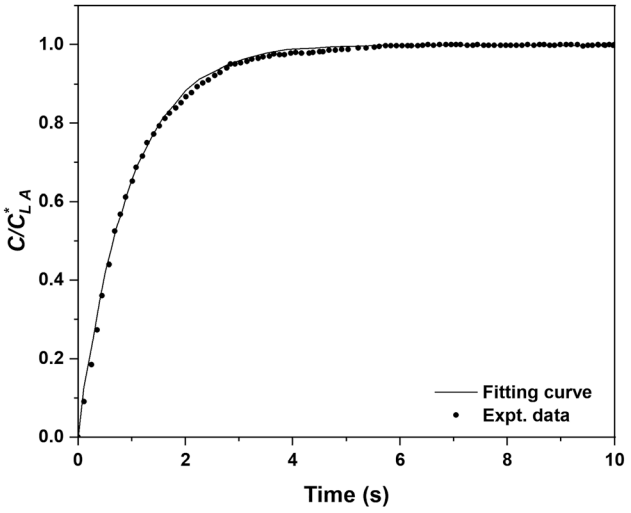

Figure 2: Response and fitting of the DO from calibration experiments.

$$\frac{dC_L}{dt} = \frac{k_L a}{\epsilon_L}\left(C^*_{L,E} - C_L\right) \tag{4}$$

Integration of the above equation with the initial conditions: $t = 0$, $C_L = C^*_{L,A}$, yields,

$$\tilde{C_L} = 1 - e^{-\left(\frac{k_L a}{\epsilon_L}\right)t} \tag{5}$$

The normalized concentration, $\tilde{C_L}$ in eq. (5) is defined as,

$$\tilde{C_L} = \frac{C_L - C^*_{L,A}}{C^*_{L,E} - C^*_{L,A}} \tag{6}$$

where $C^*_{L,A}$ and $C^*_{L,E}$ denotes the saturation concentration of oxygen in the liquid saturated by air and oxygen enriched air, respectively.

The minimum square error fit method was used to fit eq. (5) with the dissolved oxygen concentration data from the experiments to obtain $k_L a/\epsilon_L$. Then the value of $k_L a$ was computed from $k_L a/\epsilon_L$ after obtaining liquid holdup as $\epsilon_L = 1 - \epsilon_G - \epsilon_S$. The overall gas holdup, ε_G was obtained from the bed expansion studies as

$$\epsilon_G = \frac{H_d - H_s}{H_d} \tag{7}$$

where H_d, H_s are the dynamic and static bed height, respectively.

3.2 Axial dispersion model

The one-dimensional ADM for the liquid and gas phase can be written as,

$$\frac{\partial C_L}{\partial t} = D_L\frac{\partial^2 C_L}{\partial z^2} + \frac{k_L a}{\epsilon_L}\left(HC_G - C_L\right) \tag{8}$$

$$\frac{\partial C_G}{\partial t} = D_G\frac{\partial^2 C_G}{\partial z^2} - u_G\frac{\partial C_G}{\partial z} - \frac{k_L a}{\epsilon_L}\left(HC_G - C_L\right) \tag{9}$$

where H is Henry's constant, D_G, D_L are the dispersion coefficient of liquid and gas phase, respectively. The above equations were solved with the following boundary and initial conditions.

Boundary conditions:

$$z = 0, \left.\frac{\partial C_L}{\partial z}\right|_{z=0} = 0; \text{ and } u_G C_{G,\text{in}} = u_G C_G|_{z=0} - D_G\left.\frac{\partial C_G}{\partial z}\right|_{z=0}$$

$$z = L, \left.\frac{\partial C_L}{\partial z}\right|_{Z=L} = 0; \text{ and } \left.\frac{\partial C_G}{\partial z}\right|_{Z=L} = 0$$

Initial conditions: $t = 0$, $C_L = C_G = 0$.

The unknowns in eqs. (8) and (9), viz., dispersion coefficients and liquid holdup were obtained as follows. The liquid holdup was obtained as given in the previous section. Even though there will be a small variation in the liquid holdup axially, these variations are negligible in the fully developed region. The values of the gas dispersion (D_G) were obtained from the gas tracer studies in the same column with the same operating conditions, which was reported in Han, Said, and Al-Dahhan (2018). The values of the liquid dispersion for the operating conditions without solids were obtained from the virtual tracer studies of Han (2007). For the operating conditions where solids were used, dispersion coefficients of the solids were used as the liquid dispersion coefficient assuming the pseudo-homogenous slurry.

3.3 Recirculation and cross flow with dispersion (RCFD)

RCFD model considers four zones viz., upflow, downflow, bottom and top zone based on the recirculation of liquid in bubble columns (Degaleesan 1997). The upflow and downflow zones are the regions where the liquid flow is predominantly upwards (center region) and downwards (annulus region), respectively. Bottom and top zones are the regions where the flow turns, viz., sparger and disengagement region, respectively. The upward and downward zones are modeled as ADM with axial dispersion and radial dispersion between two zones. Meanwhile, sparger and disengagement zones are modeled as CSTR. RCFD model was used only for the liquid phase in this work. The gas phase has much less recirculation than the liquid, further gas phase parameters in the RCFD model are not available.

Hence, ADM was used for the gas phase. Therefore, eq. (9) and the corresponding boundary and initial conditions were used for gas phase in this case. The RCFD model equations, boundary and initial conditions for the liquid phase with mass transfer terms in SBCR are given below. The k_La values in all the four zones were assumed equal because the measurement accuracy did not support fitting different k_La values for the zones.

Upflow zone ($0 \sim r'$):

$$\frac{\partial C_{L,u}}{\partial t} = D_{z,u}\frac{\partial^2 C_{L,u}}{\partial z^2} - u_{L,u}\frac{\partial C_{L,u}}{\partial z} - \frac{4\,(D_r\epsilon_L)_{r=r'}}{r' R\epsilon_{L,u}} (C_{L,u} - C_{L,d}) + \frac{k_La}{\epsilon_{L,u}}(HC_G - C_{L,u}) \tag{10}$$

Downflow zone ($r' \sim$ R):

$$\frac{\partial C_{L,d}}{\partial t} = D_{z,d}\frac{\partial^2 C_{L,d}}{\partial z^2} + u_{L,d}\frac{\partial C_{L,d}}{\partial z} + \left(\frac{4r'/R}{R^2 - r'^2}\right)\left(\frac{(D_r\epsilon_L)_{r=r'}}{\epsilon_{L,d}}\right) \times (C_{L,u} - C_{L,d}) + \frac{k_La}{\epsilon_{L,d}}(HC_G - C_{L,d}) \tag{11}$$

Sparger zone:

$$\frac{dC_{L,a}}{dt} = \frac{\epsilon_{L,d}u_{L,d}}{\epsilon_L\phi_a D}\frac{\left(R^2 - r'^2\right)}{R^2}C_{L,d}\big|_{Z=0} - \frac{\epsilon_{L,u}u_{L,u}}{\epsilon_L\phi_a D}\frac{r'^2}{R^2}C_{L,a} + \frac{k_La}{\epsilon_L}(HC_G - C_{L,a}) \tag{12}$$

Disengagement zone:

$$\frac{dC_{L,b}}{dt} = \frac{\epsilon_{L,u}u_{L,u}}{\epsilon_L\phi_b D}\frac{r'^2}{R^2}C_{L,u}\big|_{x=L} - \frac{\epsilon_{L,d}u_{L,d}}{\epsilon_L\phi_b D}\frac{\left(R^2 - r'^2\right)}{R^2}C_{L,b} + \frac{k_La}{\epsilon_L}(HC_G - C_{L,b}) \tag{13}$$

Boundary conditions:

$$z = 0, C_{L,u}\big|_{z=0} = C_{L,a}, \quad C_{L,d}\big|_{z=0} = C_{L,a}$$

$$z = L, C_{L,u}\big|_{z=L} = C_{L,b}, \quad C_{L,d}\big|_{z=L} = C_{L,b}$$

Initial conditions: $t = 0$, $C_{L,a} = C_{L,b} = C_{L,u} = C_{L,d} = 0$.

The radial inversion point (r'), phase holdups ($\varepsilon_{L,u}$, $\varepsilon_{L,d}$) and liquid velocities ($u_{L,u}$, $u_{L,d}$) in the compartments were obtained from the computed tomography (CT) and computer aided radioactive particle tracking (CARPT) data (Han 2007). The three dispersion parameters ($D_{z,u}$, $D_{z,d}$, D_r) were obtained from the virtual tracer studies of Han (2007). The length to diameter ratio (ϕ_a, ϕ_b) of the sparger and disengagement zone was taken as 1.0 based on the CARPT results. The DO responses measured by the optical probe in the upward flowing zone ($r/R = 0$ and various axial positions) and in the downward-flowing zone ($r/R = 0.85$ and various axial positions) were fitted with $C_{L,u}$ (z, t) and $C_{L,d}$ (z, t), respectively.

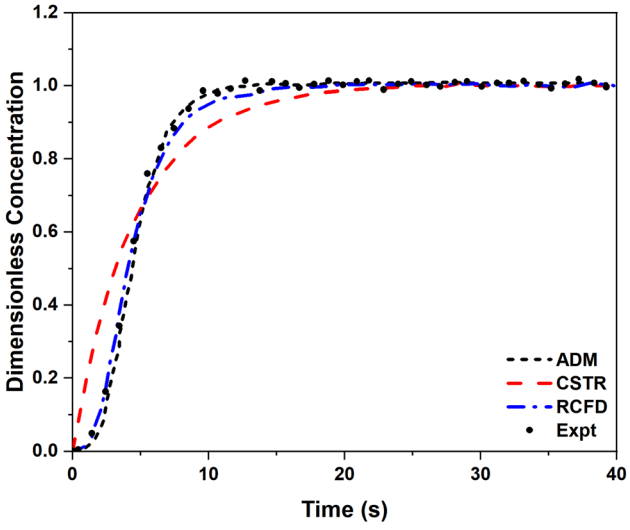

Figure 3: Comparison of concentration curves of ADM, CSTR and RCFD reactor models with experimental data at height $z/L = 0.8$ for the operating conditions of U_G – 0.3 m/s, P – 1.0 MPa. Dispersion values used for ADM are D_G – 0.135 m^2/s, D_L – 0.0764 m^2/s (Han 2007; Han, Said, and Al-Dahhan 2018). The parameters used in RCFD are $D_{z,u}$ – 0.0275 m^2/s, $D_{z,d}$ – 0.0319 m^2/s, D_r – 0.0041 m^2/s $u_{L,u}$ – 0.366 m/s, $u_{L,d}$ – 0.35 m/s (Han 2007).

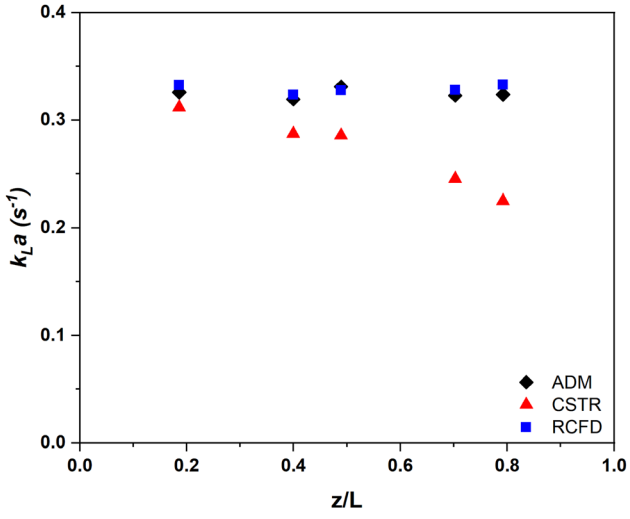

Figure 4: Comparison of volumetric mass transfer coefficient from ADM, CSTR and RCFD reactor models at different heights.

4 Results and discussion

4.1 Comparison of models

Figure 3 shows the experimental response curve fitted with the models at an axial position close to the reactor top ($z/L = 0.8$). The ADM and RCFD model have better fitting with the DO profile. Meanwhile the CSTR model gives

relatively poor fitting. The k_La values obtained using these models at different axial positions are given in Figure 4. The RCFD and ADM models gave similar results at all the axial positions. Thus, it can be concluded that using RCFD or ADM model does not lead to significant variation in the k_La values. Compared to the ADM and RCFD model, results of CSTR model are much more dependent on the axial sampling locations. The k_La values obtained using the CSTR model is 28% ($z/L = 0.8$) and 5% ($z/L = 0.2$) lower than using the ADM or RCFD model at top and bottom, respectively. Since k_La represents the overall mass transfer coefficient in the reactor model, it is expected that same k_La values would be obtained regardless of the sampling position. However, significant variation of k_La values with axial positions were obtained while using CSTR model. The k_La values at different axial sampling positions vary up to 30% while using the CSTR model, whereas the ADM or RCFD model yielded less than 5% differences. In ADM and RCFD models, the convection and dispersion of phases were accounted, whereas the CSTR model assumes uniform mixing. Hence, the differences encountered might be due to incorrect accounting of the convection and dispersion of phases. It is to be noted that Gourich et al. (2008), Manjrekar et al. (2017), Han and Al-Dahhan (2007) reported that CSTR fitting is poor due to the lack of convection term in CSTR. Contrary results were reported in the literature on axial variation of k_La while using CSTR model. Han and Al-Dahhan (2007) reported that the results vary with the height while using CSTR, whereas Chen et al. (2013) reported that there is no variation of the k_La values with the axial position. The above contrary results can be explained with the work of Gourich et al. (2008). Gourich et al. (2008) reported that if the characteristic time of the mass transfer ($1/k_La$) is more than five times of the characteristic mixing time of the gas phase ($\epsilon_G h_p/U_G$, where h_p is probe distance from the sparger), CSTR and ADM gives similar results. If the characteristic time is closer, the deviation between the CSTR and ADM increases. Physically the observation of Gourich et al. (2008) signifies that if the gas phase mixing is *significantly* faster than the mass transfer, effect of convection on the k_La is negligible. The characteristic times of Chen et al. (2013) differ by at least 10 times, thus k_La values are not significantly changing with axial position irrespective of the CSTR model used. In the case of this work and Han and Al-Dahhan (2007), characteristic time of the mass transfer is less than four times of the gas phase mixing, hence the k_La values are changing with the axial position due to the lack of the convection accounting in the CSTR model.

Unfortunately, the dispersion parameters required in ADM/RCFD models were available at a limited number of conditions only. Hence, ADM/RCFD model cannot be used for all the conditions studied in this work. From Figure 4, it can be inferred that the variation between the reactor models is reduced when measurements are made close to the inlet. However, the sampling position should not be too close to the inlet (into the sparger zone) where the gas holdup may be significantly different from the overall gas holdup (Han and Al-Dahhan 2007). Hence, the sampling position should be chosen where the influence of sparger is minimized. Degaleesan (1997) and Xue et al. (2008) reported that the sparger effect is minimized when the z/D is more than 0.7. From the computed tomography (CT) studies, Han (2007) reported that the gas holdup has not changed significantly after $z/D = 2$ at the operating conditions of this work. Based on the model comparisons, it was found that at $z/D = 2.0$ (or $z/L = 0.2$) the three reactor models yielded the smallest differences in the results (~5%). That is, at the axial position of $z/D = 0.2$, the k_La values have least dependence on the model. Hence, measurements were carried out at $z/D = 2.0$ and CSTR model was used to obtain the k_La values at all the operating conditions studied in this work.

From the above discussion, it can be concluded that it is always safer to use ADM model. For some reason CSTR model is used, applicability of model should be checked in terms of the characteristic time as observed by Gourich et al. (2008) or in terms of k_La variation with the axial position. It is be noted that the axial dependency of k_La is due to the inappropriate model used (Deckwer et al. 1983). If the applicability of the CSTR model is in question, then it is advisable to take measurements immediately after the sparger zone, where the effect of sparger is minimal. This is especially important for the studies conducted in high length-to-diameter ratio reactors.

4.2 Effect of solids loading and superficial gas velocity

The overall gas holdup obtained from eq. (7) at different superficial gas velocities and solids loadings are shown in Figure 5, corresponding k_La are given in Figure 6. The gas holdup increases with increase in the superficial gas velocity at all the pressure and solid loading conditions investigated. With increases in the gas velocity, more bubbles introduced into the reactor resulting in the higher gas holdup. However, the increase in the gas holdup is not uniform. Initially, the gas holdup increases steeply with

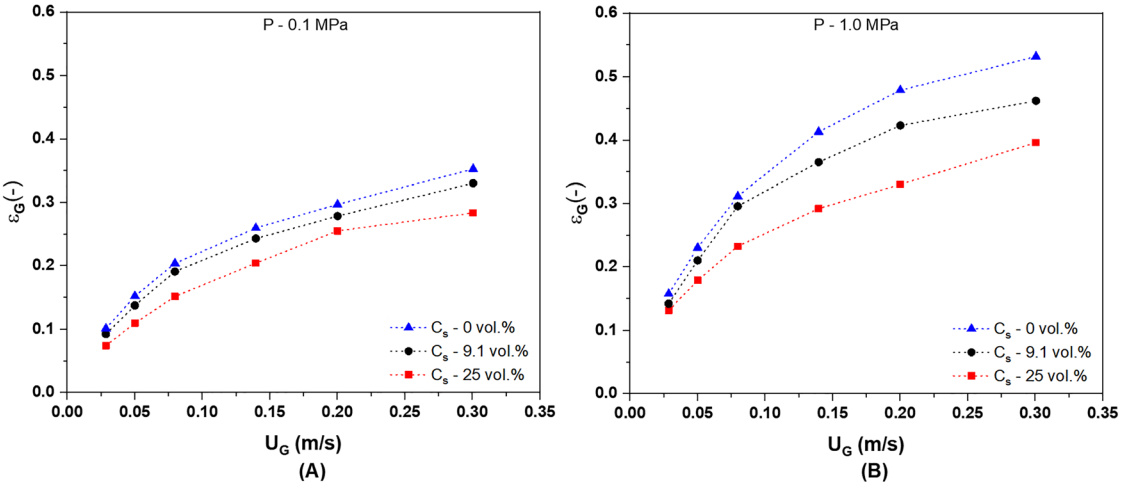

Figure 5: Effect of the superficial gas velocity and solids loading on overall gas holdup.

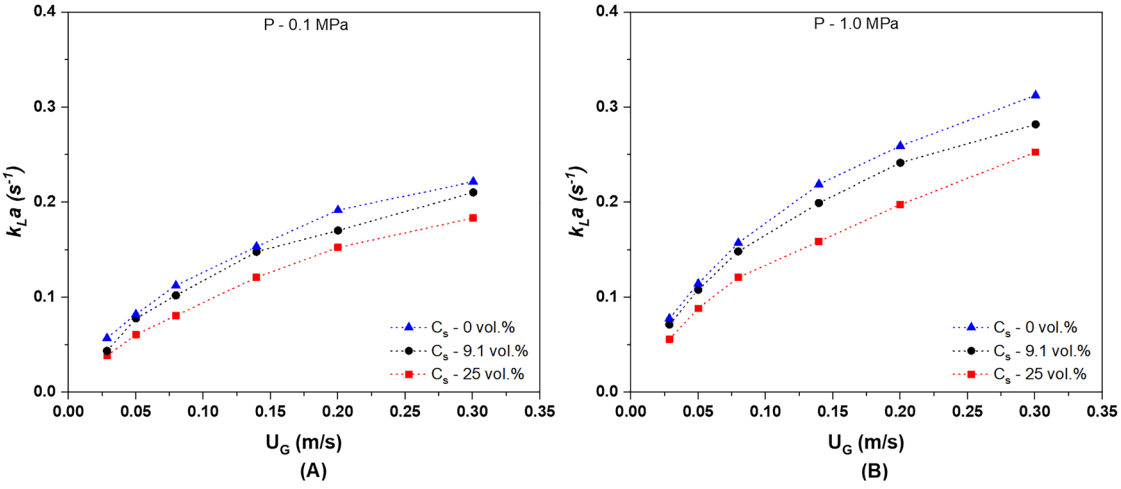

Figure 6: Effect of the superficial gas velocity and solids loading on volumetric mass transfer coefficient.

increasing in the superficial gas velocity, thereafter the slope has reduced substantially. For each conditions, the transition happens at different velocities; typically the onset happens quicker with higher solids loading. It is to be noted that similar profiles were reported by Vandu, Koop, and Krishna (2004). This change is due to the regime change from homogenous regime to heterogeneous regime. At homogenous regime, the gas holdup changes steeply due to the increase of smaller bubbles predominantly, whereas in heterogeneous regime the large bubbles were observed (Vandu, Koop, and Krishna 2004) due to coalescence, thus rate of increase of gas holdup with superficial gas velocity is reduced (Abdulkareem, Gheni, and Yacoup 2016).

The k_La is increased with the superficial gas velocity as shown in Figure 6. Increase of k_La follows the similar trend as discussed above for overall gas holdup. It is to be noted that k_La can increase due to the increase in the interfacial area or k_L. It is experimentally confirmed that the specific interfacial area follows the similar trend of the overall gas holdup and k_La of this work by Wu (2007) and Wu, Suddard and Al-Dahhan (2008). This confirms that change in the volumetric mass transfer coefficient is predominantly due to the increase in interfacial area at the investigated conditions. Similar observations has been made by Kluytmans et al. (2003), Vandu and Krishna (2004), Chen et al. (2013).

With increase in the solid loading, overall gas holdup decreases as shown in Figure 5. At higher pressure of 1.0 MPa, the decrease is more prominent compared with the lower pressure of 0.1 MPa. The viscosity of the slurry increases with the increase of solids loading, which encourages bubble coalescence resulting in the decrease of gas holdup.

Figure 6 also gives the effect of solids loading on the volumetric mass transfer coefficient. The k_La decreases at both low pressure (0.1 MPa) and high pressure (1.0 MPa) with increase in the solids loading. The trend of the k_La with the solids loading is similar to the overall gas holdup shown in Figure 5. Increasing of solids loading results in the increase of fraction of larger bubbles (thus lower gas holdup). This is also confirmed by Wu (2007). With increase in the fraction of larger bubbles, the interfacial area decreases, thus leading to the decreases of volumetric mass transfer coefficient. Similar results were reported in the previous studies of Behkish et al. (2002), Chen et al. (2013), Sehabiague and Morsi (2013). However, Vandu, Koop and Krishna (2004) reported that there is no dependence of k_La on solid loading at the similar operating conditions of this work. This might be due to the hydrodynamics disturbance while switching from nitrogen to the air in their work. Further, their work assumed that the system is well mixed and measurements were taken at the static bed height away from the distributor. From the results of this work given in Figures 3 and 4, both these assumptions affects the k_La values significantly.

4.3 Effect of operating pressure

Figure 7 shows the effect of operating pressure on the overall gas holdup. With increase in the pressure, stable bubble size decreases resulting in the larger fraction of small bubbles (Lin et al. 1998; Wilkinson 1991). The larger fraction of small bubbles increases the overall gas holdup due to the longer residence time of smaller bubbles (Lin, Tsuchiya and Fan 1998; Luo et al. 1999; Wu 2007; Xue 2004). Further, at the higher superficial gas velocity, increase of overall gas holdup with pressure is relatively high. It can also be inferred that the relative increase of overall gas holdup with pressure decreases with increase in the solid loading. This is due to the opposing effect of solids

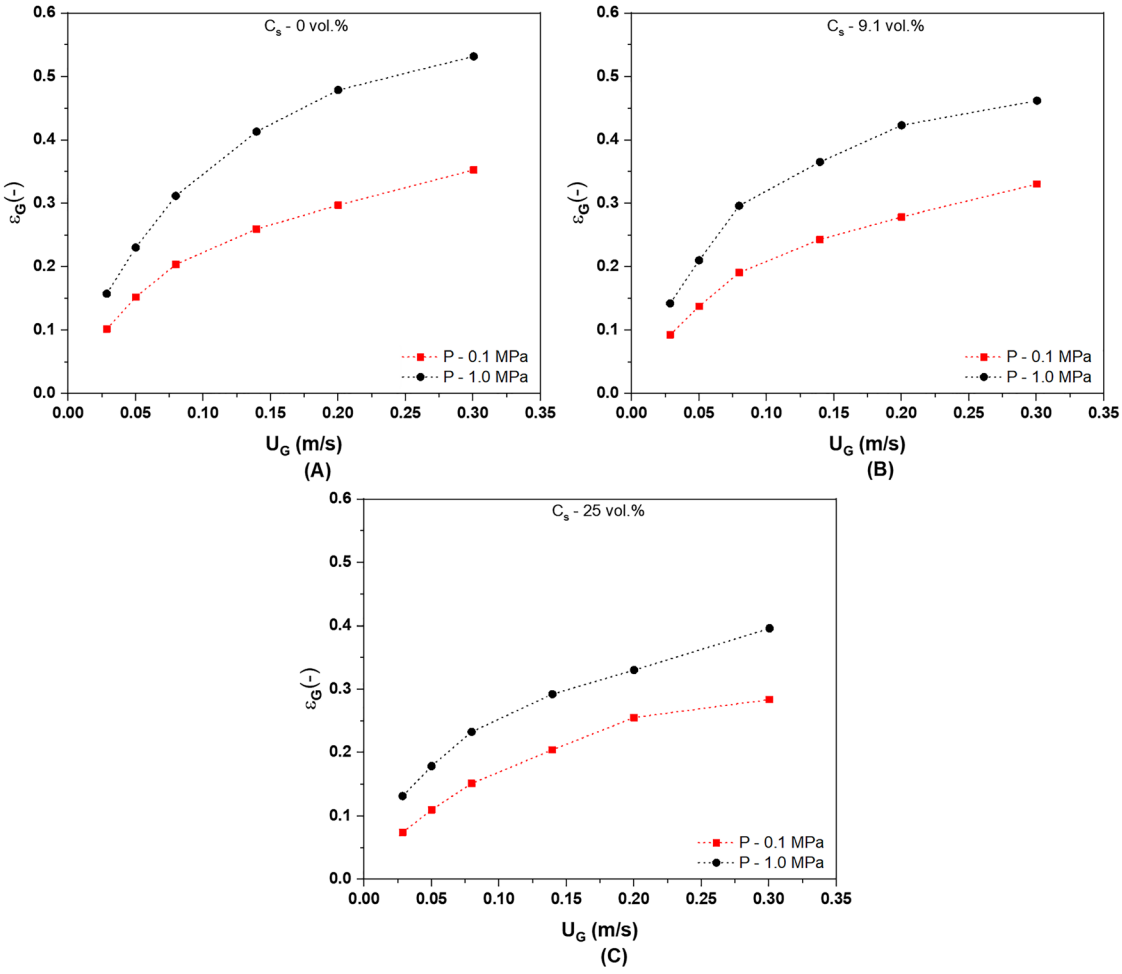

Figure 7: Effect of the operating pressure on overall gas holdup.

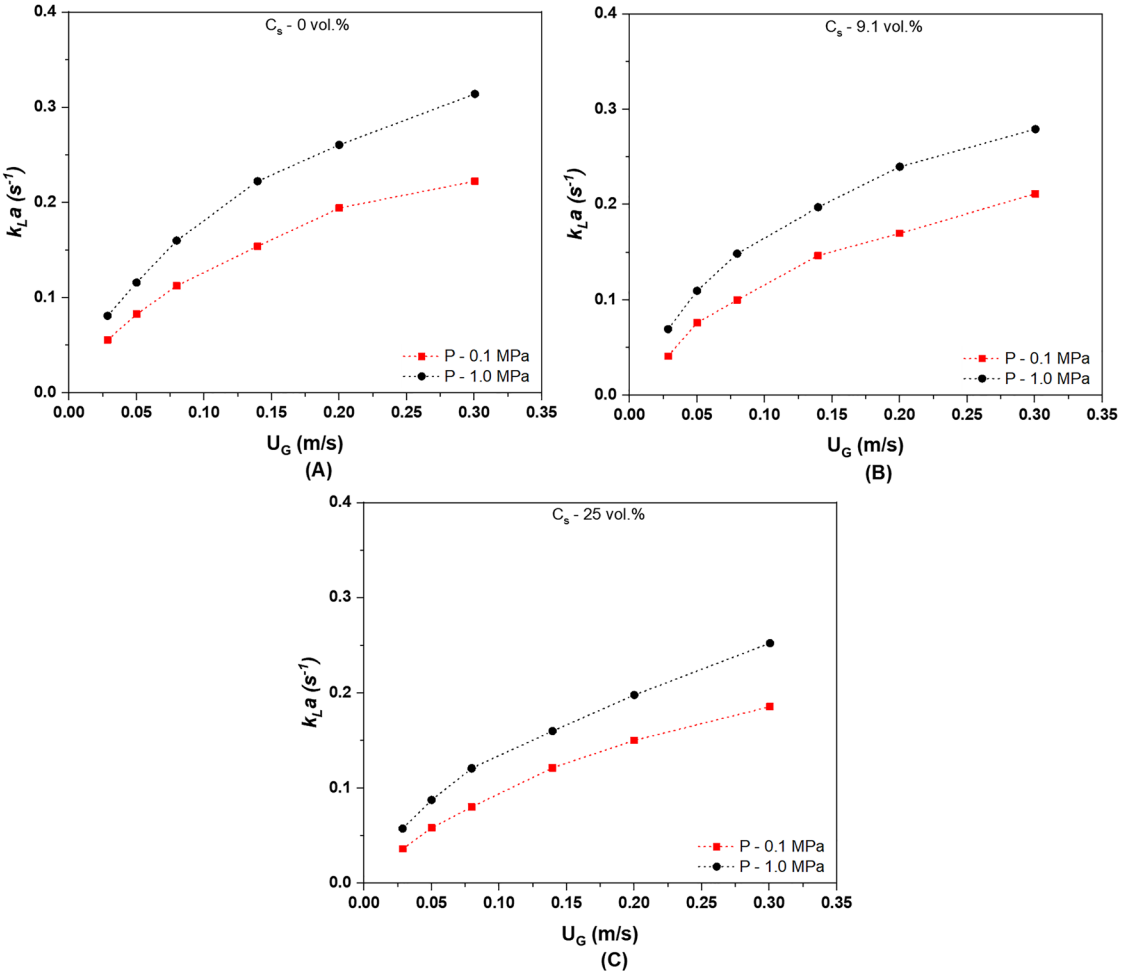

Figure 8: Effect of the operating pressure on volumetric mass transfer coefficient.

loading. The higher solids loading encourages the bubble coalescence due to the higher apparent viscosity, whereas higher pressures (higher gas density) encourages bubble breakup (Jin et al. 2014; Sehabiague and Morsi 2013). Thus, two competing phenomena results in relatively lower gas holdup at the operating conditions of this work.

Figure 8 gives the effect of operating pressure on the k_La. The k_La values increases with increase in the pressure at all the superficial gas velocity and solid loading conditions investigated. As discussed in the effect of pressure on overall gas holdup, increase in pressure leads to increase in smaller bubbles. Increases in smaller bubble results in higher gas interfacial area. This is experimentally confirmed by the work of Wu et al. (2008) at similar operating conditions in the same column. Thus, increase of volumetric mass transfer coefficient is predominately due to the increase in gas interfacial area. These observed effects of operating pressure are qualitatively similar to those observed in previous reports (Jin et al. 2014; Jordan et al. 2002; Letzel et al. 1999; Sehabiague and Morsi 2013; Yang, Wang, and Jin 2001).

5 Concluding remarks

Volumetric liquid-phase mass transfer coefficient in the mimicked FT slurry column was investigated using dissolved oxygen optical probe. The oxygen enriched air method was used, instead of conventionally used switching method to avoid the disturbance in the hydrodynamics. CSTR, ADM and RCFD models were used to find the k_La. Both ADM and RCFD model gives similar values of k_La, whereas results of CSTR model vary significantly from the other models and depend on the axial position. From the literature and this work, it can be concluded that it is always safe to use ADM model. If the CSTR model is used, the applicability of the model should be checked and the sampling should be done at the axial

position immediately after the sparger zone. With increase in the operating pressure and superficial velocity, k_La increases, while with solid loading it decreases. From the results, it can be referred that change of k_La is prominently due to the change in the interfacial area at the studied conditions.

Nomenclature

a	Gas–liquid interfacial area, m^2 Sparger zone
C_L, C_G	Concentration of oxygen in liquid and gas phase, respectively, $kmol/m^3$
$C_{L,a}$, $C_{L,b}$	Concentration of oxygen in liquid phase in the upflow and downflow zone, respectively, $kmol/m^3$
$C_{L,u}$, $C_{L,d}$	Concentration of oxygen in liquid phase in the sparger and disengagement zone, respectively, $kmol/m^3$
C_p	Concentration of oxygen measured by DO probe, $kmol/m^3$
C_s	Solids loading, vol%
$C^*_{L,A}$	Saturation concentration of oxygen in the liquid saturated by air, $kmol/m^3$
$C^*_{L,E}$	Saturation concentration of oxygen in the liquid saturated by oxygen enriched air, $kmol/m^3$
$\tilde{C}_L$	Normalized concentration, –
D	Diameter of the column, m
D_G, D_L	Dispersion coefficient of gas and liquid phase, respectively, m^2/s
$D_{z,u}$, $D_{z,d}$	Axial dispersion coefficient of liquid in the upflow and downflow zone, respectively, m^2/s
D_r	Radial dispersion coefficient of liquid, m^2/s
H	Henry's constant
H_d, H_s	Height of dynamic and static bed, respectively, m
k_p	Probe constant, s^{-1}
k_La	Volumetric mass transfer coefficient, s^{-1}
P	Pressure, MPa
r'	Radial inversion point, m
R	Radius of the column, m
t	Time, s
T	Temperature, K
U_G	Superficial gas velocity, m/s

Greek letters

ε	Holdup
ϕ	Length to diameter ratio

Subscripts

a	Sparger zone
A	Air
b	Disengagement zone
d	Downflow zone
E	Oxygen enriched air
G	Gas
L	Liquid
p	DO probe
S	Solids
u	Upflow zone

Acknowledgments: The authors would like to acknowledge the financial support of members of High Pressure Slurry Bubble Column (HPSBC) consortium - ConocoPhillips (USA), EniTechnologie (Italy), Sasol (South Africa) and Statoil (Norway).

Author contributions: All the authors have accepted responsibility for the entire content of this submitted manuscript and approved submission.

Research funding: None declared.

Conflict of interest statement: The authors declare no conflicts of interest regarding this article.

References

Abdulkareem, H. A., S. A. Gheni, and R. J. Yacoup. 2016. "Study of the Hydrodynamics and Mass Transfer Coefficient in a 2D Mimicked FT Slurry Bubble Columns for Alternative Clean Energy and Chemical Production." *International Journal of Chemical Reactor Engineering* 14 (5): 975–90.

Basha, O. M., L. Sehabiague, A. Abdel-wahab, and B. I. Morsi. 2015. "Fischer–Tropsch Synthesis in Slurry Bubble Column Reactors: Experimental Investigations and Modeling – A Review." *International Journal of Chemical Reactor Engineering* 13 (3): 201–88.

Behkish, A., Z. Men, J. R. Inga, and B. I. Morsi. 2002. "Mass Transfer Characteristics in a Large-Scale Slurry Bubble Column Reactor with Organic Liquid Mixtures." *Chemical Engineering Science* 57 (16): 3307–24.

Chang, H. N., B. Halard, and M. Moo-Young. 1989. "Measurement of k_La by a Gassing-In Method with Oxygen-Enriched Air." *Biotechnology and Bioengineering* 34: 1147–57.

Chen, P., P. Gupta, M. P. Dudukovic, and B. A. Toseland. 2006. "Hydrodynamics of Slurry Bubble Column During Dimethyl Ether (DME) Synthesis: Gas–Liquid Recirculation Model and Radioactive Tracer Studies." *Chemical Engineering Science* 61 (19): 6553–70.

Chen, Z., H. Liu, H. Zhang, W. Ying, and D. Fang. 2013. "Oxygen Mass Transfer Coefficient in Bubble Column Slurry Reactor with Ultrafine Suspended Particles and Neural Network Prediction." *The Canadian Journal of Chemical Engineering* 91 (3): 532–41.

Deckwer, W. D., Y. Loulsl, A. Zaldl, and M. Ralek. 1980. "Hydrodynamic Properties of the Fischer–Tropsch Slurry Process." *Industrial & Engineering Chemistry Process Design and Development* 19 (4): 699–708.

Deckwer, W. D., K. Nguyen-Tien, B. G. Kelkar, and Y. T. Shah. 1983. "Applicability of Axial Dispersion Model to Analyze Mass-Transfer Measurements in Bubble Columns." *AIChE Journal* 29 (6): 915–22.

Degaleesan, S. 1997. *Fluid Dynamic Measurements and Modeling of Liquid Mixing in Bubble Columns*. St. Louis, Missouri, USA: Washington University.

Degaleesan, S., S. Roy, B. Kumar, and M. P. Duduković. 1996. "Liquid Mixing Based on Convection and Turbulent Dispersion in Bubble Columns." *Chemical Engineering Science* 51 (10): 1967–76.

Ghani, S. A., R. J. Yaqub, and S. S. Saleh. 2012. "Experimental Study of Volumetric Mass Transfer Coefficients in Slurry Bubble Column Reactor." *Journal of Chemical Engineering & Process Technology* 3 (3): 10–13.

Gourich, B., C. Vial, N. El Azher, M. B. Soulami, and M. Ziyad. 2008. "Influence of Hydrodynamics and Probe Response on Oxygen Mass Transfer Measurements in a High Aspect Ratio Bubble Column Reactor: Effect of the Coalescence Behaviour of the Liquid Phase." *Biochemical Engineering Journal* 39: 1–14.

Gupta, P., M. H. Al-Dahhan, M. P. Dudukovic, and B. A. Toseland. 2001. "Comparison of Single- and Two-Bubble Class Gas – Liquid Recirculation Models – Application to Pilot-Plant Radioactive Tracer Studies during Methanol Synthesis." *Chemical Engineering Science* 56: 1117–25.

Han, L. 2007. *Hydrodynamics, Back-Mixing, and Mass Transfer in a Slurry Bubble Column Reactor for Fischer–Tropsch Alternative Fuels*. St. Louis, Missouri, USA: Washington University.

Han, L., and M. H. Al-Dahhan. 2007. "Gas–Liquid Mass Transfer in a High Pressure Bubble Column Reactor with Different Sparger Designs." *Chemical Engineering Science* 62 (1–2): 131–9.

Han, L., I. Said, and M. H. Al-Dahhan. 2018. "Gas Phase Back-Mixing in a Mimicked Fischer–Tropsch Slurry Bubble Column Using an Advanced Gaseous Tracer Technique." *International Journal of Chemical Reactor Engineering* 17 (2): 1–14.

Jin, H., S. Yang, G. He, D. Liu, Z. Tong, and J. Zhu. 2014. "Gas–Liquid Mass Transfer Characteristics in a Gas–Liquid–Solid Bubble Column Under Elevated Pressure and Temperature." *Chinese Journal of Chemical Engineering* 22 (9): 955–61.

Jordan, U., K. Terasaka, G. Kundu, and A. Schumpe. 2002. "Mass Transfer in High-Pressure Bubble Columns with Organic Liquids." *Chemical Engineering and Technology* 25 (3): 262–5, https://doi.org/10.1002/1521-4125(200203)25:3<262::aid-ceat262>3.0.co;2-c.

Kluytmans, J. H. J., B. G. M. van Wachem, B. F. M. Kuster, and J. C. Schouten. 2003. "Mass Transfer in Sparged and Stirred Reactors: Influence of Carbon Particles and Electrolyte." *Chemical Engineering Science* 58 (20): 4719–28.

Lau, R., W. Peng, G. Q. Yang, and L. Fan. 2004. "Gas–Liquid Mass Transfer in High-Pressure Bubble Columns." *Industrial & Engineering Chemistry Research* 43 (5): 1302–11.

Letzel, H. M., J. C. Schouten, R. Krishna, and C. M. van den Bleek. 1999. "Gas Holdup and Mass Transfer in Bubble Column Reactors Operated at Elevated Pressure." *Chemical Engineering Science* 54 (13–14): 2237–46.

Li, X., and C. Zhu. 2016. "Gas–Liquid Mass Transfer with Instantaneous Chemical Reaction in a Slurry Bubble Column Containing Fine Reactant Particles." *Chemical Industry and Chemical Engineering Quarterly* 22 (1): 85–93.

Lin, T.-J., K. Tsuchiya, and L. S. Fan. 1998. "Bubble Flow Characteristics in Bubble Columns at Elevated Pressure and Temperature." *AIChE Journal* 44 (3): 545–60.

Linek, V., J. Sinkule, and P. Benes. 1991. "Critical Assessment of Gassing-In Methods for Measuring k_La in Fermentors." *Biotechnology and Bioengineering* 38: 323–30.

Luo, X., D. J. Lee, R. Lau, G. Yang, and L. S. Fan. 1999. "Maximum Stable Bubble Size and Gas Holdup in High-Pressure Slurry Bubble Columns." *AIChE Journal* 45 (4): 655–80.

Manjrekar, O. N., Y. Sun, L. He, Y. J. Tang, and M. P. Dudukovic. 2017. "Hydrodynamics and Mass Transfer Coefficients in a Bubble Column Photo-Bioreactor." *Chemical Engineering Science* 168: 55–66.

Sehabiague, L., and B. I. Morsi. 2013. "Hydrodynamic and Mass Transfer Characteristics in a Large-Scale Slurry Bubble Column Reactor for Gas Mixtures in Actual Fischer–Tropsch Cuts." *International Journal of Chemical Reactor Engineering* 11 (1): 1–20.

Shaikh, A. 2007. *Bubble and Slurry Bubble Column Reactors for Syngas to Liquid Fuel Conversion: Mixing, Flow Regime Transition, and Scale-Up*. St. Louis, Missouri, USA: Washington University.

Vandu, C. O., and R. Krishna. 2004. "Volumetric Mass Transfer Coefficients in Slurry Bubble Columns Operating in the Churn-Turbulent Flow Regime." *Chemical Engineering and Processing* 43: 987–95.

Vandu, C. O., K. Koop, and R. Krishna. 2004. "Volumetric Mass Transfer Coefficient in a Slurry Bubble Column Operating in the Heterogeneous Flow Regime." *Chemical Engineering Science* 59: 5417–23.

Vandu, C. O., B. van den Berg, and R. Krishna. 2005. "Gas–Liquid Mass Transfer in a Slurry Bubble Column at High Slurry Concentrations and High Gas Velocities." *Chemical Engineering and Technology* 28: 998–1002.

Wei, Y., Y. Jiao, D. An, D. Li, W. Li, and Q. Wei. 2019. "Review of Dissolved Oxygen Detection Technology: From Laboratory Analysis to Online Intelligent Detection." *Sensors* 19: 3995.

Wilkinson, P. M. 1991. *Physical Aspects and Scale-Up of High Pressure Bubble Columns*. Rijksuniversiteit Groningen, The Netherlands: University of Groningen.

Wu, C. 2007. *Heat Transfer and Bubble Dynamics in Slurry Bubble Columns for Fischer–Tropsch Clean Alternative Energy*. St. Louis, Missouri, USA: Washington University.

Wu, C., K. Suddard, and M. H. Al-Dahhan. 2008. "Bubble Dynamics Investigation in a Slurry Bubble Column." *AIChE Journal* 54 (5): 1203–12.

Xue, J. 2004. *Bubble Velocity, Size and Interfacial Area Measurements in Bubble Columns*. St. Louis, Missouri, USA: Washington University.

Xue, J., M. H. Al-Dahhan, M. P. Dudukovic, and R. F. Mudde. 2008. "Bubble Velocity, Size, and Interfacial Area Measurements in a Bubble Column by Four-Point Optical Probe." *AIChE Journal* 54 (2): 350–63.

Yang, B. W., J. Wang, and Y. Jin. 2001. "Mass Transfer Characteristics of Syngas Components in Slurry System at Industrial Conditions." *Chemical Engineering and Technology* 24 (6): 651–7, https://doi.org/10.1002/1521-4125(200106)24:6<651::aid-ceat651>3.0.co;2-x.

Zhang, Y., L. Chen, Z. Lin, L. Ding, X. Zhang, R. Dai, Q. Yan, and X. Wang. 2019. "Highly Sensitive Dissolved Oxygen Sensor with a Sustainable Antifouling, Antiabrasion, and Self-Cleaning Superhydrophobic Surface." *ACS Omega* 4: 1715–21.